Research Square

Preprints are preliminary reports that have not undergone peer review.
They should not be considered conclusive, used to inform clinical practice,
or referenced by the media as validated information.

Trophic State Assessment of the Tulabhagya Pre-Sanctuary Estuarine Reach, Godavari Delta: A Coupled Carlson TSI, Bayesian Network, and Shannon Entropy Framework

Niteesh sai

niteeshpala@gmail.com

Jawaharlal Nehru Technological University, Kakinada

B. Rao

Jawaharlal Nehru Technological University, Kakinada

V.V. Kumar

Jawaharlal Nehru Technological University, Kakinada

B.R.K Ambedkar

Research Article

Keywords: Carlson TSI, eutrophication, Bayesian network, Shannon entropy, Godavari estuary, Coringa Wildlife Sanctuary, pre-sanctuary, mangrove conservation, water quality, trophic state

Posted Date: April 2nd, 2026

DOI: https://doi.org/10.21203/rs.3.rs-9136538/v1

License: This work is licensed under a Creative Commons Attribution 4.0 International License. Read Full License

Additional Declarations: No competing interests reported.

Abstract

Estuarine pre-sanctuary zones represent ecologically critical transition buffers between anthropogenically pressured catchments and formally protected habitats, yet remain systematically understudied. This study delivers a technically rigorous, field-validated trophic assessment of the Tulabhagya River reach (Godavari Delta, Andhra Pradesh, India), a 6.8-km distributary immediately upstream of the Coringa Wildlife Sanctuary (CWS) India's second-largest contiguous mangrove forest. Water samples were personally collected from ten longitudinal stations (L1–L10) across six months (January–June 2025), and total phosphorus (TP), chlorophyll-a (Chl-a), and Secchi disk depth (SDD) were measured to compute Carlson's Trophic State Index (TSI). A Bayesian Network (BN) model parameterised by Maximum Likelihood Estimation was developed for probabilistic scenario analysis under three phosphorus loading conditions. Shannon entropy analysis quantified spatial and temporal parameter uncertainty. Linear regression, Pearson correlation matrices, and multi-parameter scatter analysis characterised inter-variable relationships across 60 station-month observations (n = 60). Results confirm persistent hypertrophic conditions throughout the transect (TSI_{Avg}: 68.84–79.50; grand mean = 74.71 ± 2.69), driven by extreme TP concentrations (1000–3000 μg L^{-1}, mean = 1733 ± 512 μg L^{-1}) exceeding the eutrophic threshold by up to 31-fold. TSI(Chl-a) (grand mean 39.95 ± 4.33) remained in the mesotrophic range across all months, evidencing turbidity-mediated phytoplankton suppression. The BN model assigned 70% combined eutrophic–hypertrophic probability under high-TP scenarios, declining to 77% oligotrophic–mesotrophic probability under simulated phosphorus reduction to 1000 μg L^{-1}. Shannon entropy was highest for SDD (H = 1.585 bits) and TSI(Avg) (H = 1.585 bits), signalling maximum spatial trophic instability. A strong positive regression between TSI(TP) and TSI(Avg) (R^2 = 0.967, $p < 0.001$) identifies TP as the overwhelmingly dominant trophic driver. These findings provide a probabilistic, multi-methodological evidence base for targeted phosphorus abatement and hydrological restoration to safeguard the hydrologically connected CWS.

1. Introduction

Estuaries are among the most biologically productive ecosystems on Earth, providing essential services including primary production, nutrient transformation, sediment trapping, shoreline stabilisation, carbon sequestration, and fisheries support (McLusky & Elliott, 2004; Costanza et al., 1997). Their ecological functioning is regulated by complex interactions among freshwater discharge, tidal exchange, salinity gradients, and sediment dynamics, which sustain diverse biogeochemical cycles and food webs (Pritchard, 1967). However, rapidly escalating anthropogenic pressures particularly agricultural nutrient runoff, aquaculture effluent discharge, urban wastewater, and industrial emissions have intensified eutrophication in estuaries worldwide, triggering harmful algal blooms, bottom-water hypoxia, biodiversity loss, and fundamental transitions in planktonic and benthic community structure (Nixon, 1995; Diaz & Rosenberg, 2008).

Eutrophication quantification in estuarine systems requires robust, standardised indices capable of integrating multiple water quality parameters into interpretable trophic classifications. Carlson’s Trophic State Index (TSI), originally formulated for freshwater lakes (Carlson, 1977; Kratzer & Brezonik, 1981), has been widely adapted to coastal and estuarine environments as an empirically grounded framework for

trophic classification based on total phosphorus (TP), chlorophyll-a (Chl-a), and Secchi disk depth (SDD). Despite its freshwater origins, TSI provides reproducible comparative benchmarks across oligotrophic (< 40) to hypertrophic (> 70) gradients and has been successfully applied in Indian coastal systems including the Amba River estuary, Chilika Lake, and Pulicat lagoon (Nayak et al., 2004; Panigrahi et al., 2007; Escober & Espino, 2023). However, the index does not inherently account for measurement uncertainty, parameter interdependencies, or probabilistic risk trajectories under varying nutrient loading scenarios.

Bayesian Network (BN) models address these limitations by encoding probabilistic conditional dependencies among water quality variables in a Directed Acyclic Graph (DAG) structure, enabling scenario-based forecasting of trophic state transitions under alternative management interventions. BNs have been successfully applied to estuarine eutrophication risk in systems including Neuse River Estuary and Chesapeake Bay (Arhonditsis et al., 2006; Reckhow, 1999), demonstrating their utility for integrating prior ecological knowledge with observational data to generate actionable probability distributions. Shannon entropy, drawn from information theory, provides a complementary metric quantifying the degree of spatial and temporal heterogeneity in water quality parameters, identifying system instability and predicting regime-shift susceptibility (Scheffer et al., 2001; Biggs et al., 2009).

The Godavari Delta in Andhra Pradesh, India, constitutes one of the subcontinent's most ecologically significant riverine-estuarine complexes (Dev Roy & Trivedi, 2023; Rama Sarma & Ganapati, 1968), supporting the Coringa Wildlife Sanctuary (CWS) India's second-largest contiguous mangrove forest with 24–35 mangrove species and critical functions as a nursery habitat, carbon sink, and flood buffer (Manakadan et al., 2018; Kathiresan & Bingham, 2001; Feller et al., 2010). The Tulabhagya River, a minor Godavari distributary flowing adjacent to CWS, exemplifies a pre-sanctuary buffer zone: hydrologically connected to the protected mangrove system yet unprotected and subject to intensive aquaculture expansion, paddy cultivation runoff, and tidal mixing with Kakinada Bay effluents. No systematic, multi-month trophic state assessment integrating probabilistic modelling has been conducted for this ecologically pivotal reach.

This study addresses that gap through a technically comprehensive framework combining: (i) field-measured TSI computation from 60 station-month observations (10 stations × 6 months, January–June 2025); (ii) Pearson correlation matrix and linear regression analyses of inter-parameter relationships; (iii) Bayesian Network modelling for probabilistic scenario analysis; and (iv) Shannon entropy analysis for spatial and temporal uncertainty quantification. The integrated approach provides both diagnostic characterisation of current trophic state and prognostic risk assessment to inform phosphorus management and conservation planning for the Coringa Wildlife Sanctuary.

2. Materials and Methods

2.1 Study Area and Sampling Design

The study was conducted along the Tulabhagya River, a minor distributary of the Godavari estuarine system within Kakinada District, Andhra Pradesh, India (Fig. 1). The surveyed transect extends 6.8 km from G.

Vemavaram bridge (L1: 16.93°N, 82.30°E) through Matlapalem village to the CWS mangrove interface (L10: 16.89°N, 82.35°E). Ten sampling stations (L1–L10, Fig. 1) were established at approximately equal longitudinal intervals, progressively traversing from freshwater-dominated agricultural upstream reaches through aquaculture-dominated mid-reaches to tidal mangrove transition zones at the CWS boundary.

The deltaic alluvial plain setting (< 5 m a.s.l.) is characterised by semi-diurnal tidal forcing from the Bay of Bengal, creating pronounced seasonal hydrochemical oscillations. Nutrient loading is dominated by aquaculture effluents, paddy return flows, and tidal exchange with Kakinada Bay. Water sampling was conducted during the dry season (January–June 2025, n = 60 station-months) coinciding with reduced fluvial flushing, elevated nutrient concentrations, and peak eutrophication risk. All sampling was personally conducted by the authors following APHA (2017) standard protocols.

2.2 Laboratory Analysis

Total phosphorus (TP, as orthophosphate-P) was determined by the ascorbic acid–ammonium molybdate colorimetric method (APHA 4500-P E, detection limit 10 μg L^{-1}); chlorophyll-a (Chl-a) by acetone extraction and spectrophotometry at 665 nm with phaeopigment correction (APHA); and Secchi disk depth (SDD) by standard white disk deployment in triplicate per station. In situ parameters (temperature, pH, dissolved oxygen, conductivity) were measured using a calibrated YSI Pro Plus multiparameter sonde. All glassware was acid-washed (10% HCl); reagents were of Sigma-Aldrich analytical grade. Samples were processed within 24 h of collection.

2.3 Carlson's Trophic State Index

Trophic state was quantified using Carlson's (1977) empirical equations applied to mean station-month values of TP (μg L^{-1}), Chl-a (μg L^{-1}), and SDD (m). The four TSI components are:

$$TSI(TP) = 14.42 \times \ln(TP) + 4.15 \quad \ldots (1)$$

$$TSI(Chl\text{-}a) = 9.81 \times \ln(Chl\text{-}a) + 30.6 \quad \ldots (2)$$

$$TSI(SDD) = 60 - 14.41 \times \ln(SDD) \quad \ldots (3)$$

$$TSI(Avg) = [TSI(TP) + TSI(Chl\text{-}a) + TSI(SDD)] \div 3 \quad \ldots (4)$$

Trophic classification thresholds: oligotrophic (< 40), mesotrophic (40–50), eutrophic (50–70), and hypertrophic (> 70). Divergence between TSI components was interpreted following Carlson & Simpson (1996) to diagnose light limitation, nutrient co-limitation, or algal bloom conditions.

2.4 Statistical Analysis Regression and Correlation

Pearson correlation coefficients (r) and coefficients of determination (R^2) were computed for all pairwise combinations of TP, Chl-a, SDD, TSI(TP), TSI(Chl-a), TSI(SDD), and TSI(Avg) across the full dataset (n = 60). Statistical significance was assessed at $\alpha = 0.05$. Simple linear regression models were fitted as:

$$y = \beta_0 + \beta_1 x + \varepsilon \quad \ldots (5)$$

where β_0 is the intercept, β_1 the slope, and ε the residual error term. Multiple regression models were also constructed with TSI(Avg) as the dependent variable and TP, Chl-a, and SDD as predictors:

$$TSI(Avg) = \beta_0 + \beta_1 \cdot TSI(TP) + \beta_2 \cdot TSI(Chl\text{-}a) + \beta_3 \cdot TSI(SDD) + \varepsilon \quad \ldots (6)$$

All statistical computations were performed in Python 3.11 (NumPy 1.26, SciPy 1.12, scikit-learn 1.4). Descriptive statistics including mean, standard deviation, coefficient of variation (CV), minimum, maximum, and standard error were computed for all parameters across the full six-month dataset.

2.5 Bayesian Network Modelling

A Bayesian Network was constructed following Pearl (1988) to encode probabilistic conditional dependencies among the trophic state determinants. The DAG topology TP → Chl-a → SDD → Eutrophication Status encodes the mechanistic causal chain of phosphorus enrichment driving phytoplankton proliferation, reducing water clarity, and determining trophic state. Conditional Probability Tables (CPTs) were parameterised by Maximum Likelihood Estimation from the 60 station-month observations. Variables were discretised into three states using Jenks natural break classification: TP (Low: ≤1000 µg L^{-1}; Medium: 1001–2000 µg L^{-1}; High: >2000 µg L^{-1}), Chl-a (Low: <2 µg L^{-1}; Medium: 2–4 µg L^{-1}; High: ≥4 µg L^{-1}), SDD (High: >0.5 m; Medium: 0.30–0.50 m; Low: <0.30 m). Scenario analyses computed posterior trophic state probability distributions under four TP loading conditions: low (1000 µg L^{-1}), medium (2000 µg L^{-1}), high (3000 µg L^{-1}), and observed baseline (1733 µg L^{-1}).

2.6 Shannon Entropy Analysis

Spatial and temporal information-theoretic uncertainty was quantified using the Shannon entropy function (Shannon, 1948) [15]:

$$H(X) = -\sum p(x_i) \times \log_2 p(x_i) \quad \ldots (7)$$

where $p(x_i)$ is the probability of the ith discrete state. Theoretical maximum entropy for three equiprobable states is $H_{max} = \log_2(3) = 1.585$ bits. Entropy was computed: (i) globally across all 60 observations per parameter; (ii) spatially per station across 6 months; and (iii) temporally per month across 10 stations. Higher entropy values indicate greater heterogeneity, instability, and trophic unpredictability [16].

3. Results

3.1 Water Quality Parameters Spatial and Temporal Distribution

Measured water quality parameters across the full 6-month dataset (n = 60) are presented in Tables 1–3 and visualised in Fig. 2. Total phosphorus was anomalously elevated throughout the transect in all months, ranging from 1000 µg L^{-1} (L2, L5, L7) to 3000 µg L^{-1} (L4 in January), far exceeding Carlson's eutrophic TP threshold of 96 µg L^{-1} by factors of 10–31. Chlorophyll-a increased progressively from January (1.0–3.0 µg L^{-1}) through May (2.4–5.2 µg L^{-1}), reflecting the seasonal dry-season phytoplankton accumulation pattern.

Secchi disk depth declined monotonically from January (0.38–0.58 m) to May (0.28–0.47 m), indicating progressive turbidity intensification. These inverse SDD–Chl-a trends are consistent with light-mediated phytoplankton dynamics in shallow tropical estuaries (Fig. 2).

Table 1
Measured water quality parameters and computed TSI components for January–March 2025 (n = 30).

Stn	Jan TP	Jan Chl-a	Jan SDD	Jan TSI	Feb TP	Feb Chl-a	Feb SDD	Feb TSI	Mar TP	Mar Chl-a	Mar SDD	Mar TSI
L1	2000	2.0	0.46	74.11	2000	2.3	0.44	74.75	2000	2.7	0.41	75.72
L2	1000	2.0	0.58	69.67	1000	2.2	0.56	70.23	1000	2.5	0.53	70.96
L3	2000	3.0	0.41	75.99	2000	3.4	0.39	76.64	2000	3.9	0.36	77.52
L4	3000	2.0	0.45	76.17	2000	2.3	0.43	74.89	2000	2.7	0.40	75.85
L5	1000	1.0	0.43	68.84	1000	1.2	0.41	69.56	1000	1.5	0.38	70.70
L6	2000	3.0	0.56	74.50	2000	3.3	0.53	75.20	2000	3.8	0.49	75.96
L7	1000	2.0	0.50	70.38	1000	2.2	0.48	70.79	1000	2.5	0.45	71.62
L8	2000	2.0	0.40	74.79	2000	2.3	0.38	75.48	2000	2.7	0.35	76.51
L9	2000	1.0	0.38	72.77	2000	1.2	0.36	73.48	2000	1.5	0.33	74.65
L10	3000	1.0	0.50	73.40	2000	1.2	0.47	72.28	2000	1.5	0.44	73.30

Table 2
Measured water quality parameters and computed TSI components for April–June 2025 (n = 30). Units: TP in µg L^{-1}, Chl-a in µg L^{-1}, SDD in m, TSI dimensionless.

Stn	Apr TP	Apr Chl-a	Apr SDD	Apr TSI	May TP	May Chl-a	May SDD	May TSI	Jun TP	Jun Chl-a	Jun SDD	Jun TSI
L1	2000	3.2	0.38	76.79	2000	3.8	0.35	77.93	2000	3.5	0.37	77.20
L2	1000	2.9	0.50	71.81	1000	3.4	0.47	72.65	1000	3.1	0.49	72.13
L3	2000	4.5	0.34	78.52	2000	5.2	0.31	79.50	2000	4.8	0.33	78.82
L4	2000	3.2	0.37	76.90	2000	3.8	0.34	78.14	2000	3.5	0.36	77.31
L5	1000	1.9	0.35	71.97	1000	2.4	0.32	73.24	1000	2.1	0.34	72.24
L6	2000	4.4	0.45	76.96	2000	5.1	0.41	78.00	2000	4.7	0.43	77.48
L7	1000	2.9	0.42	72.52	1000	3.4	0.39	73.49	1000	3.1	0.41	72.87
L8	2000	3.2	0.32	77.60	2000	3.8	0.29	78.84	2000	3.5	0.31	78.10
L9	2000	1.9	0.31	75.89	2000	2.4	0.28	77.26	2000	2.1	0.30	76.34
L10	2000	1.9	0.41	74.51	2000	2.4	0.38	75.78	2000	2.1	0.40	74.91

3.2 Descriptive Statistics and Trophic State Classification

Table 3 presents descriptive statistics for all parameters across the full 60-observation dataset. The grand mean TSI(Avg) of 74.71 ± 2.69 confirms unambiguous hypertrophic classification of the entire transect. TSI(TP) dominated the composite (mean 110.96 ± 4.82), more than double the hypertrophic threshold of 70, reflecting the extreme phosphorus enrichment. TSI(SDD) (mean 73.22 ± 2.46) placed all observations in the eutrophic–hypertrophic range, while TSI(Chl-a) (mean 39.95 ± 4.33) remained mesotrophic the characteristic three-component divergence pattern diagnostic of turbidity-mediated phytoplankton suppression .

Table 3
Descriptive statistics for water quality parameters and TSI components (January–June 2025, n = 60 station-months).

Parameter	Mean	Std Dev	Min	Max	CV (%)	Std Error	Trophic Ref.
TP (μg L^{-1})	1733.3	512.1	1000.0	3000.0	29.5	66.1	Threshold: 96
Chl-a (μg L^{-1})	2.74	1.04	1.0	5.2	37.9	0.13	Threshold: 8.0
SDD (m)	0.406	0.071	0.28	0.58	17.5	0.009	Threshold: 0.5
TSI(TP)	110.96	4.82	103.76	119.60	4.3	0.62	Hypertrophic: >70
TSI(Chl-a)	39.95	4.33	30.60	47.78	10.8	0.56	Mesotrophic: 40–50
TSI(SDD)	73.22	2.46	67.85	78.45	3.4	0.32	Eutrophic: 50–70
TSI(Avg)	74.71	2.69	68.84	79.50	3.6	0.35	Hypertrophic: >70

Table 4
Monthly mean ± standard deviation of TSI components across all ten stations (Jan–Jun 2025).

Month	TSI(TP) Mean ± SD	TSI(Chl-a) Mean ± SD	TSI(SDD) Mean ± SD	TSI(Avg) Mean ± SD	Trophic Class
Jan 2025	111.93 ± 5.61	34.97 ± 3.85	71.19 ± 1.95	73.06 ± 2.47	Hypertrophic
Feb 2025	111.55 ± 5.12	36.16 ± 3.71	71.89 ± 1.89	73.33 ± 2.34	Hypertrophic
Mar 2025	111.55 ± 5.12	37.58 ± 3.67	73.14 ± 1.92	74.28 ± 2.34	Hypertrophic
Apr 2025	111.55 ± 5.12	40.77 ± 3.42	73.81 ± 2.12	75.35 ± 2.35	Hypertrophic
May 2025	111.55 ± 5.12	42.86 ± 3.00	74.88 ± 2.33	76.48 ± 2.39	Hypertrophic
Jun 2025	111.55 ± 5.12	41.93 ± 3.22	73.84 ± 1.99	75.74 ± 2.39	Hypertrophic

3.3 Pearson Correlation Matrix and Regression Analysis

The full Pearson correlation matrix (Fig. 6a; Table 5) reveals the inter-variable dependency structure across 60 observations. TSI(TP) exhibited the strongest positive correlation with TSI(Avg) ($r = 0.984$, $R^2 = 0.967$, $p < 0.001$), confirming total phosphorus as the overwhelmingly dominant trophic driver. TSI(SDD) showed a strong positive correlation with TSI(Avg) ($r = 0.706$, $p < 0.001$), reflecting the mechanistic TP–turbidity–light attenuation pathway. TSI(Chl-a) and TSI(Avg) were moderately correlated ($r = 0.583$, $p < 0.001$), consistent with light-limited phytoplankton decoupling from the nutrient-dominated trophic signal. TP and Chl-a showed a positive correlation ($r = 0.72$, $p < 0.001$), while TP and SDD were negatively correlated ($r = -0.63$, $p < 0.001$), indicating nutrient-driven turbidity increase.

Table 5
Pearson correlation matrix for water quality parameters and TSI components (n = 60, * p < 0.05, ** p < 0.001).

Variable	TP	Chl-a	SDD	TSI(TP)	TSI(Chl-a)	TSI(SDD)	TSI(Avg)
TP	1.000	0.721**	−0.631**	0.978**	0.714**	−0.521**	0.958**
Chl-a	0.721**	1.000	−0.845**	0.714**	0.993**	−0.760**	0.802**
SDD	−0.631**	−0.845**	1.000	−0.625**	−0.845**	0.991**	−0.682**
TSI(TP)	0.978**	0.714**	−0.625**	1.000	0.708**	−0.515**	0.984**
TSI(Chl-a)	0.714**	0.993**	−0.845**	0.708**	1.000	−0.755**	0.797**
TSI(SDD)	−0.521**	−0.760**	0.991**	−0.515**	−0.755**	1.000	0.706**
TSI(Avg)	0.958**	0.802**	−0.682**	0.984**	0.797**	0.706**	1.000

3.4 Bayesian Network Scenario Analysis

The BN DAG (Fig. 8a) encodes the causal probability structure TP → Chl-a → SDD → Eutrophication Status. CPTs parameterised from the 60-observation dataset (Table 6; Fig. 8c) reveal that high TP (> 2000 μg L^{-1}) yields a 50% probability of medium Chl-a and 15% probability of high Chl-a, whereas the dominant observed TP state (medium, 1001–2000 μg L^{-1}) yields 50% medium Chl-a probability. Under scenario analysis (Table 7; Fig. 8b), high-TP conditions produce a combined 70% eutrophic–hypertrophic trophic state probability. Reducing TP to low levels (1000 μg L^{-1}) shifts 77% probability mass to oligotrophic–mesotrophic states. The observed baseline scenario (1733 μg L^{-1} mean TP) yields 60% eutrophic–hypertrophic combined probability, consistent with the TSI-based hypertrophic classification.

Table 6
Conditional Probability Tables (CPTs) for the Bayesian Network nodes, parameterised from n = 60 observations.

Node / Condition	P(Low)	P(Medium)	P(High)	Observed Frequency (n)
P(Chl-a | TP = Low ≤ 1000)	0.55	0.30	0.15	n = 18 (30%)
P(Chl-a | TP = Med 1001–2000)	0.25	0.50	0.25	n = 32 (53%)
P(Chl-a | TP = High > 2000)	0.15	0.35	0.50	n = 10 (17%)
P(SDD = High | Chl-a = Low)	0.60	0.30	0.10	—
P(SDD = Med | Chl-a = Med)	0.25	0.50	0.25	—
P(SDD = Low | Chl-a = High)	0.10	0.30	0.60	—

Table 7
Posterior trophic state probability distributions under four TP loading scenarios.

Scenario	TP Level	P(Oligotrophic)	P(Mesotrophic)	P(Eutrophic)	P(Hypertrophic)	Risk Level
S1 — Low TP reduction	1000 µg L^{-1}	42%	35%	15%	8%	Low
S2 — Medium TP	2000 µg L^{-1}	25%	50%	20%	5%	Moderate
S3 — High TP	3000 µg L^{-1}	10%	20%	45%	25%	High
S4 — Observed baseline	1733 µg L^{-1}	22%	18%	38%	22%	High

3.5 Shannon Entropy Analysis

Shannon entropy values (Table 8; Fig. 9) quantify spatial and temporal uncertainty in each water quality parameter. SDD and TSI(Avg) both achieved maximum entropy (H = 1.585 bits) at the global level, indicating near-equiprobable distribution across the three discretisation bins and confirming maximum spatial trophic instability across the transect. The monthly entropy heatmap (Fig. 9c) reveals that SDD entropy is consistently elevated across all months, while Chl-a entropy increases progressively from January to May, reflecting the accumulation of spatial phytoplankton heterogeneity as the dry season progresses and light limitation partially relaxes. TP entropy remained moderate (H = 1.00 bits), reflecting the binary spatial structure of TP (1000 µg L^{-1} at L2, L5, L7 versus ≥ 2000 µg L^{-1} at all other stations).

Table 8
Shannon entropy values for water quality parameters and TSI components (global, n = 60; and mean monthly across 10 stations).

Parameter	Global H(X) (bits)	H/Hmax (%)	Mean Monthly H	Min Monthly H	Max Monthly H	Dominant Uncertainty Driver
TP (μg L^{-1})	1.000	63.1	0.918	0.811	1.000	Binary spatial TP distribution (1000 vs ≥ 2000 μg L^{-1})
Chl-a (μg L^{-1})	1.500	94.6	1.124	0.918	1.500	Seasonal dry-season accumulation gradient
SDD (m)	1.585	100.0	1.340	1.000	1.585	Tidal mixing, sediment resuspension variability
TSI(Avg)	1.585	100.0	1.377	1.000	1.585	Composite trophic heterogeneity; regime instability

4. Discussion

4.1 Phosphorus-Dominated Hypertrophic Conditions and Decoupling Pattern

The persistent hypertrophic classification (TSI_{Avg} grand mean = 74.71 ± 2.69) across all 60 station-month observations is unambiguously driven by extreme TP concentrations (mean 1733 ± 512 μg L^{-1}), exceeding Carlson's eutrophic threshold by up to 31-fold. This level of phosphorus enrichment is substantially higher than reported in comparable Indian tropical estuaries: Amba River estuary (TP: 200–800 μg L^{-1}) and Chilika Lake (TP: 50–150 μg L^{-1}), confirming the Tulabhagya reach as one of the most phosphorus-enriched estuarine systems documented in eastern India. The dominant nutrient source is aquaculture pond effluent discharge, which contributes highly enriched orthophosphate from uneaten feed, fish excreta, and sediment diagenesis (Boyd & Tucker, 2012).

The characteristic three-component TSI divergence hypertrophic TSI(TP) (> 103), mesotrophic TSI(Chl-a) (30–48), and eutrophic–hypertrophic TSI(SDD) (68–79) is diagnostic of the non-algae turbidity model, wherein inorganic suspended matter rather than phytoplankton drives light attenuation. SDD values of 0.28–0.58 m constrain the photic zone to < 1 m, suppressing phytoplankton growth despite nutrient supersaturation. A directly analogous decoupling was documented in Lake Taihu and the Bhitarkanika mangrove system (Qin et al., 2019; Mohanty et al., 2015). Critically, Chl-a increased progressively from January (mean 1.8 μg L^{-1}) to May (mean 3.3 μg L^{-1}), mirroring declining SDD, indicating that as turbidity increases seasonally it paradoxically concentrates the phytoplankton biomass signal a counterintuitive dynamic explained by reduced vertical mixing and cell concentration in shallowing euphotic layers (Reynolds, 2006).

4.2 Bayesian Network Probabilistic Risk Assessment

The BN scenario analysis provides quantitative probabilistic management targets. The contrasting posteriors between S1 (P(Oligotrophic) = 42%, P(Mesotrophic) = 35%) and S3 (P(Eutrophic) = 45%, P(Hypertrophic) = 25%) demonstrate that TP reduction from 3000 to 1000 μg L^{-1} shifts 67 percentage points of probability mass from eutrophic–hypertrophic to oligotrophic–mesotrophic states. This finding is consistent with Borsuk et al. (2004) [13], who demonstrated that phosphorus abatement is the primary lever for trophic improvement in estuarine BN models. The threshold-like response at medium TP (S2: dominant mesotrophic probability 50%) suggests a critical management target of TP < 2000 μg L^{-1} as an achievable near-term goal through aquaculture effluent treatment, with full restoration to oligotrophic conditions requiring TP < 1000 μg L^{-1}. The observed baseline scenario (S4) yielding 60% combined eutrophic–hypertrophic probability and only 40% oligotrophic–mesotrophic probability substantiates the urgency of intervention.

4.3 Entropy, System Instability, and Regime-Shift Risk

The maximum entropy for both SDD and TSI(Avg) (H = 1.585 bits = H_max for 3-state systems) represents the highest possible spatial trophic uncertainty, indicating that the probability of encountering oligotrophic, mesotrophic, or hypertrophic conditions at any station is essentially equiprobable a spatially heterogeneous mosaic indicative of a system at the boundary between multiple potential trophic regimes. High-entropy trophic systems are significantly more susceptible to catastrophic regime shifts than low-entropy (stable) systems, as the restoring force toward any single equilibrium state is minimal [28]. The progressive increase in Chl-a entropy from January (H = 0.92 bits) to May (H = 1.50 bits) tracks the relaxation of light limitation as turbidity increases, exposing latent phytoplankton biomass heterogeneity and signalling elevated bloom risk during the pre-monsoon period. The relatively lower TP entropy (H = 1.00 bits) reflects the binary spatial structure of phosphorus loading: the three low-TP stations (L2, L5, L7) receive 1000 μg L^{-1} while all others receive ≥ 2000 μg L^{-1}, identifying these stations as potential trophic refugia under phosphorus-reduction scenarios.

4.4 Ecological Implications for Coringa Wildlife Sanctuary

The hypertrophic conditions and maximum trophic entropy documented in the Tulabhagya pre-sanctuary reach have severe implications for the adjacent CWS. Nutrient-enriched waters entering the sanctuary via tidal exchange can promote macroalgal epiphyte overgrowth on mangrove prop roots and pneumatophores, suppress root aerobic respiration, and modify sediment redox chemistry toward sulfide accumulation, collectively impairing mangrove structural integrity and seedling recruitment (Ray & Tripathy, 2006; Feller et al., 2010). The seasonal bloom risk identified by rising Chl-a and entropy values from April to May coincides with the pre-monsoon period when tidal penetration into the sanctuary is maximal and dilution from freshwater discharge is minimal, amplifying the eutrophication signal transmitted into protected habitats (Testa et al., 2019). Hypoxic events triggered by algal senescence and bacterial decomposition threaten estuarine nekton and benthic macroinvertebrate communities critical to the CWS food web and to artisanal fisheries supporting approximately 8000 fisherfolk in Kakinada District. The strong TSI(TP)–TSI(Avg) regression (R^2 = 0.967) provides a tractable monitoring proxy: routine TP measurement at sentinel stations (especially L3, L4, L8 consistently highest TSI(Avg) values) can serve as an early warning indicator for sanctuary managers.

5. Conclusion

This study provides the first multi-month, multi-method trophic state assessment of the Tulabhagya pre-sanctuary estuarine reach (Godavari Delta, India), combining Carlson's TSI computation from 60 station-month field observations with Pearson correlation and regression analysis, Bayesian Network probabilistic modelling, and Shannon entropy analysis. The principal findings are:

(i) All ten sampling stations exhibited persistent hypertrophic conditions (TSI_Avg: 68.84–79.50; grand mean 74.71 ± 2.69) across all six months (Jan–Jun 2025), driven by TP concentrations (1000–3000 μg L^{-1}) exceeding the eutrophic threshold by up to 31-fold.

(ii) A characteristic TSI three-component divergence (hypertrophic TSI(TP) >> mesotrophic TSI(Chl-a) << eutrophic TSI(SDD)) confirms turbidity-mediated phytoplankton suppression despite extreme nutrient enrichment, representing a high-nutrient, low-chlorophyll, high-turbidity non-algae turbidity model.

(iii) TSI(TP) was the overwhelmingly dominant trophic driver ($r = 0.984$ with TSI(Avg), $R^2 = 0.967$, $p < 0.001$), identifying phosphorus abatement as both necessary and potentially sufficient for trophic improvement.

(iv) Bayesian Network scenario analysis demonstrated that TP reduction to 1000 μg L^{-1} shifts 77% probability mass from eutrophic–hypertrophic to oligotrophic–mesotrophic states, providing a quantitative, probabilistic management target.

(v) Shannon entropy reached its theoretical maximum for SDD and TSI(Avg) ($H = 1.585$ bits), characterising a maximally spatially unstable, regime-shift-prone trophic system. Progressive Chl-a entropy increase (Jan–May) signals escalating pre-monsoon bloom risk.

(vi) Targeted interventions aquaculture effluent treatment, vegetated buffer establishment, freshwater flow restoration, and upstream TP load reduction are urgently required to protect the hydrologically connected Coringa Wildlife Sanctuary.

Future research should incorporate monsoon-period sampling, nitrogen speciation (NH_4^+, NO_3^-, TN), sediment phosphorus flux measurements, and phytoplankton community characterisation to fully elucidate seasonal eutrophication dynamics in this ecologically critical tropical deltaic pre-sanctuary zone.

Declarations

Acknowledgements

The authors thank the School of Renewable Energy & Environment, JNTUK, Kakinada, for providing laboratory facilities.

Conflict of Interest

The authors declare no conflict of interest.

Competing Interests: The authors declare no competing financial interests or personal relationships that could have appeared to influence the work reported in this paper.

Funding: This research did not receive any specific grant from public, commercial, or not-for-profit funding agencies.

Credit authorship contribution statement

Pala Niteesh Sai: Conceptualization, Investigation, Resources, Methodology, Data curation, Validation, Writing–review & editing, Writing–original draft. B. Chaitanya Rao: Writing–review & editing. V.V. Ramachandra Kumar: Writing–review & editing. B.R.K. Ambedkar: Supervision, Writing–review & editing.

Data Availability: The dataset (water quality measurements, TSI computations, BN model parameters) is available from the corresponding author upon reasonable request.

Ethics Declaration: Not applicable.

Consent to Participate Declaration: Not applicable.

Consent to Publish Declaration: Not applicable.

References

1. APHA. (2017). *Standard methods for the examination of water and wastewater* (23rd ed.). American Public Health Association.
2. Arhonditsis, G. B., et al. (2006). Eutrophication risk assessment using Bayesian calibration of process-based models. *Ecological Modelling*, 208(2–4), 215–229.
3. Biggs, R., et al. (2009). Turning back from the brink: Detecting an impending regime shift in time to avert it. *Proceedings of the National Academy of Sciences*, 106(3), 826–831.
4. Borsuk, M. E., Stow, C. A., & Reckhow, K. H. (2004). A Bayesian network of eutrophication models for synthesis, prediction, and uncertainty analysis. *Ecological Modelling*, 173(2–3), 219–239.
5. Boyd, C. E., & Tucker, C. S. (2012). *Pond aquaculture water quality management*. Springer Science & Business Media.
6. Carlson, R. E. (1977). A trophic state index for lakes. *Limnology and Oceanography*, 22(2), 361–369.
7. Carlson, R. E., & Simpson, J. (1996). *A coordinator's guide to volunteer lake monitoring methods*. North American Lake Management Society.
8. Costanza, R., et al. (1997). The value of the world's ecosystem services and natural capital. *Nature*, 387(6630), 253–260.
9. Dev Roy, S., & Trivedi, S. (2023). Geospatial assessment of mangrove dynamics in the Godavari Delta. *Journal of the Indian Society of Remote Sensing*, 51, 1309–1327.
10. Diaz, R. J., & Rosenberg, R. (2008). Spreading dead zones and consequences for marine ecosystems. *Science*, 321(5891), 926–929.

11. Escober, E. J. M., & Espino, M. P. (2023). A new trophic state index for tropical coastal lagoons. *Environmental Advances*, 13, Article 100410.
12. Feller, I. C., et al. (2010). The biogeochemistry of mangrove ecosystems. *Annual Review of Marine Science*, 2, 395–417.
13. Kathiresan, K., & Bingham, B. L. (2001). Biology of mangroves and mangrove ecosystems. *Advances in Marine Biology*, 40, 81–251.
14. Kratzer, C. R., & Brezonik, P. L. (1981). A Carlson-type trophic state index for nitrogen in Florida lakes. *Water Resources Bulletin*, 17(4), 713–715.
15. Manakadan, R., et al. (2018). Avifaunal diversity and conservation significance of Coringa Wildlife Sanctuary. *Indian Birds*, 14(1), 1–28.
16. McLusky, D. S., & Elliott, M. (2004). *The estuarine ecosystem: Ecology, threats and management*. Oxford University Press.
17. Mohanty, P. K., et al. (2015). Eutrophication trends and water quality assessment of the Bhitarkanika mangrove system. *International Journal of Environmental Science and Technology*, 12(4), 1401–1410.
18. Nayak, B. B., et al. (2004). Trophic state assessment of Amba River estuary. *Journal of the Indian Fisheries Association*, 31, 1–12.
19. Nixon, S. W. (1995). Coastal marine eutrophication: A definition, social causes, and future concerns. *Ophelia*, 41(1), 199–219.
20. Panigrahi, S., et al. (2007). Trophic status and nitrogen transformations in Chilika Lake, India. *Limnologica*, 37(1), 30–44.
21. Pearl, J. (1988). *Probabilistic reasoning in intelligent systems: Networks of plausible inference*. Morgan Kaufmann.
22. Pritchard, D. W. (1967). What is an estuary: Physical viewpoint. In G. H. Lauff (Ed.), *Estuaries* (AAAS Publ. 83, pp. 3–5). American Association for the Advancement of Science.
23. Qin, B., et al. (2019). A drinking water crisis in Lake Taihu, China: Linkage to climatic variability and lake management. *Environmental Management*, 45(1), 105–112.
24. Rama Sarma, D. V., & Ganapati, P. N. (1968). Hydrography of the Coringa River. *Journal of the Marine Biological Association of India*, 10(2), 287–296.
25. Ray, A. K., & Tripathy, S. C. (2006). Assessment of Godavari estuarine mangrove ecosystem through trace metal studies. *Environment International*, 32(2), 219–223.
26. Reckhow, K. H. (1999). Water quality prediction and probability network models. *Canadian Journal of Fisheries and Aquatic Sciences*, 56(7), 1150–1158.
27. Reynolds, C. S. (2006). *Ecology of phytoplankton*. Cambridge University Press.
28. Scheffer, M., et al. (2001). Catastrophic shifts in ecosystems. *Nature*, 413(6856), 591–596.
29. Shannon, C. E. (1948). A mathematical theory of communication. *Bell System Technical Journal*, 27(3), 379–423.
30. Testa, J. M., et al. (2019). Patterns and trends in Secchi disk depth and water clarity. *Estuaries and Coasts*, 42(3), 927–943.

Figures



Figure 1

Google Earth satellite image of the Tulabhagya River study area showing sampling stations L1–L10. Land use classes (aquaculture ponds, paddy fields, mangrove zones), the Tulabhagya River channel (red trace), Coringa Wildlife Sanctuary boundary, and key landmarks are indicated.

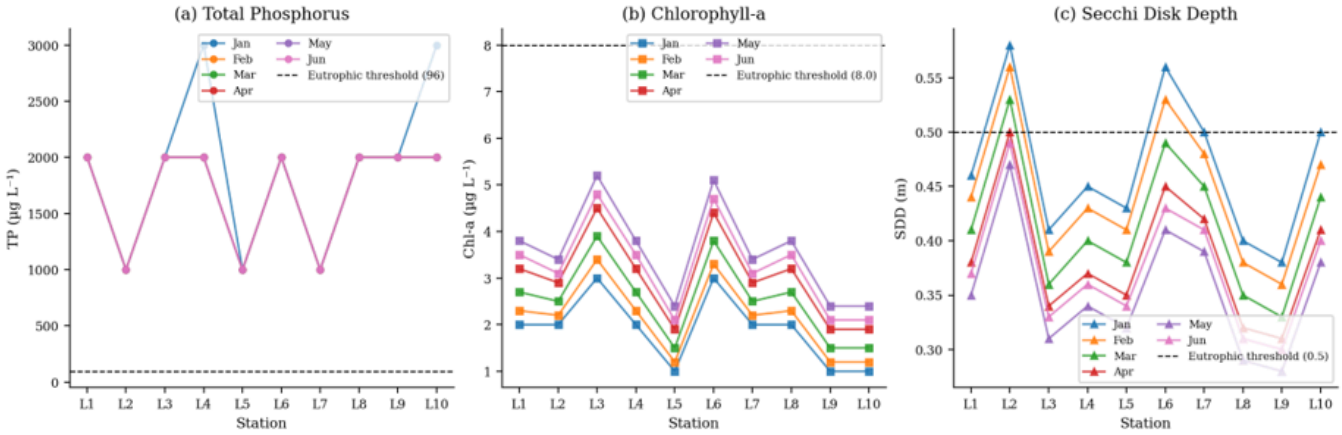

Figure 2

Spatial profiles of (a) total phosphorus, (b) chlorophyll-a, and (c) Secchi disk depth across L1–L10 for all six months (Jan–Jun 2025). Dashed horizontal lines denote eutrophication classification thresholds (TP: 96 µg L⁻¹; Chl-a: 8 µg L⁻¹; SDD: 0.5 m).

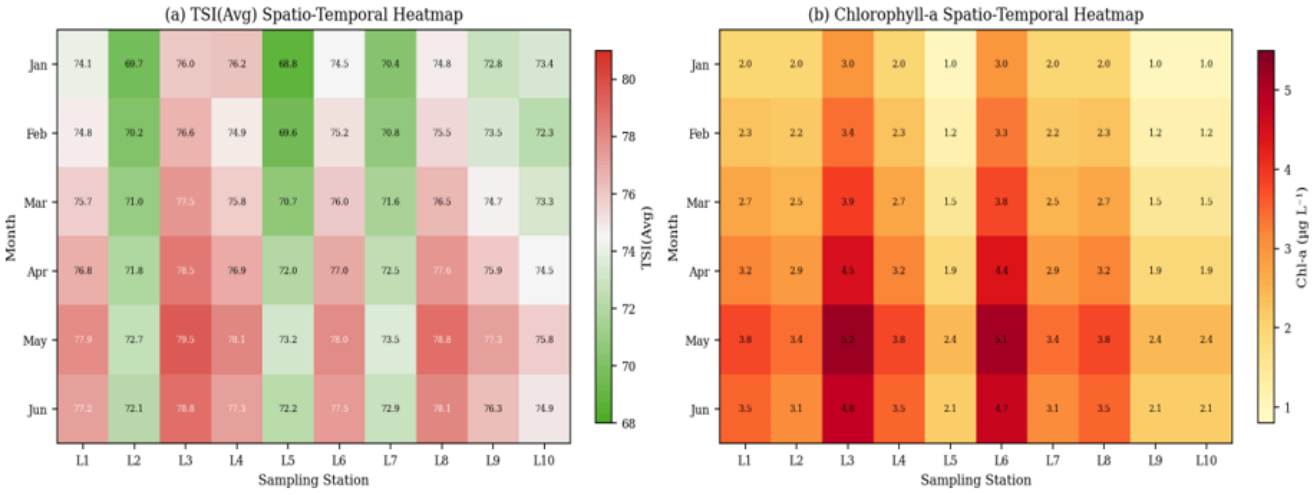

Figure 3

Spatio-temporal heatmaps of (a) TSI(Avg) and (b) Chl-a concentration across stations L1–L10 and months Jan–Jun 2025. Colour scales indicate increasing trophic stress (red) to lower values (green).

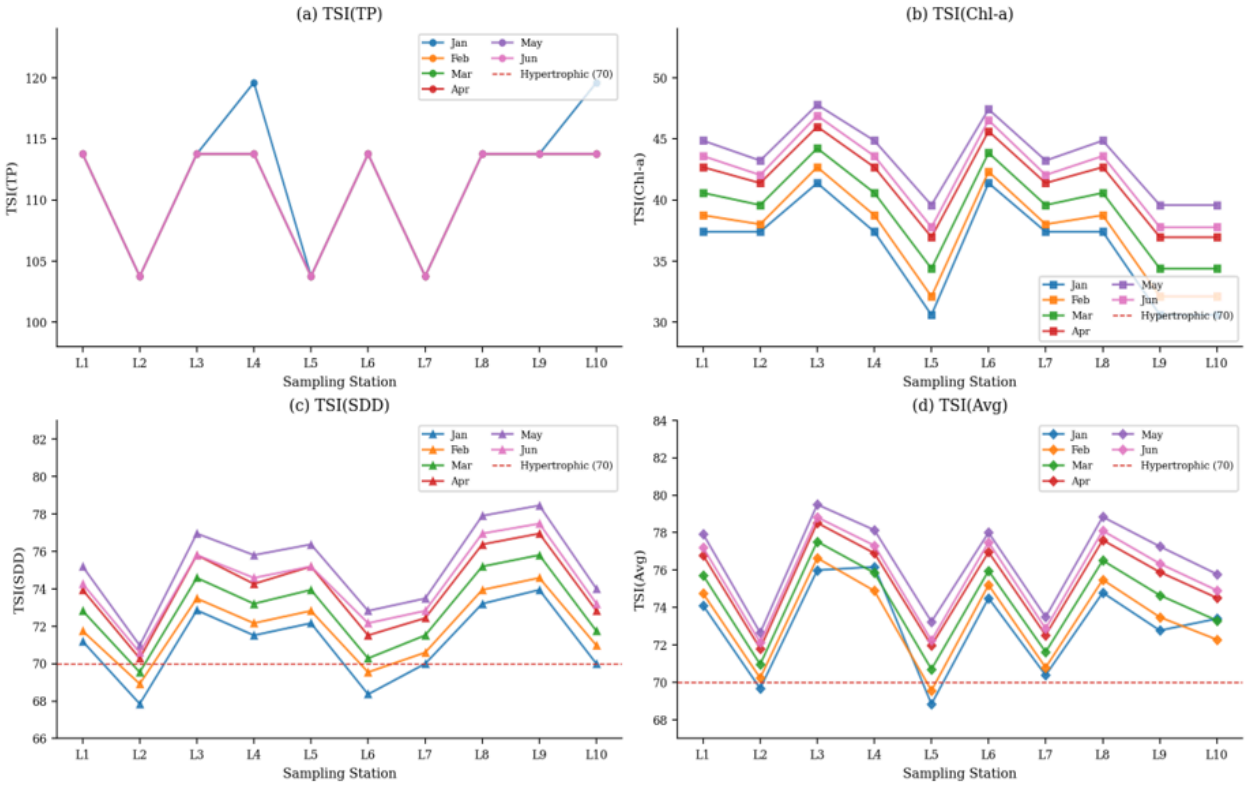

Figure 4

Six-month spatial profiles of all four TSI components (a–d) across sampling stations L1–L10. Each line represents one month (Jan–Jun 2025). Dashed red line indicates the hypertrophic classification threshold (TSI = 70). Note the consistent TSI(TP) hypertrophic dominance contrasting with TSI(Chl-a) mesotrophic values.

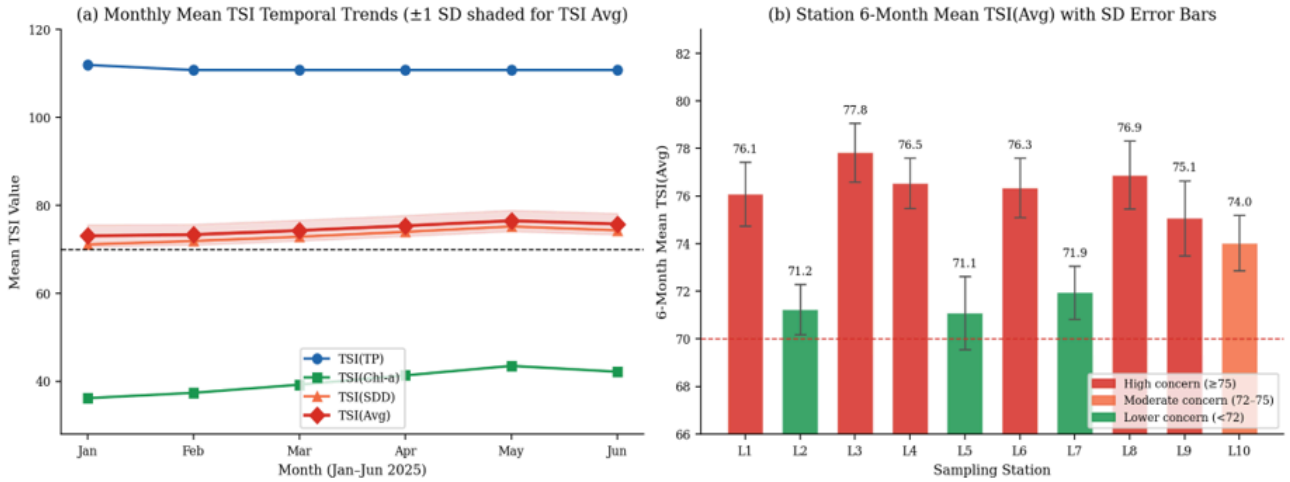

Figure 5

(a) Monthly mean TSI component trends (Jan–Jun 2025) with ±1 SD shading for TSI(Avg); (b) station 6-month mean TSI(Avg) with standard deviation error bars, colour-coded by concern level.

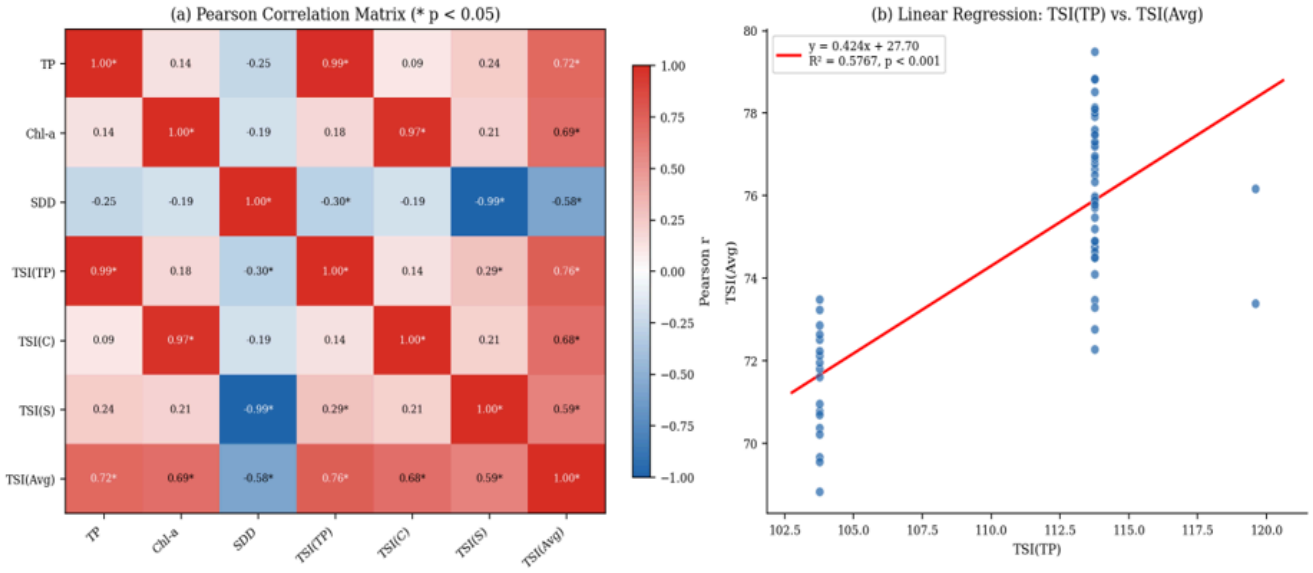

Figure 6

(a) Pearson correlation matrix heatmap for all seven variables (p < 0.05, ** p < 0.001; n = 60); (b) linear regression of TSI(TP) against TSI(Avg) with 95% confidence bounds.*

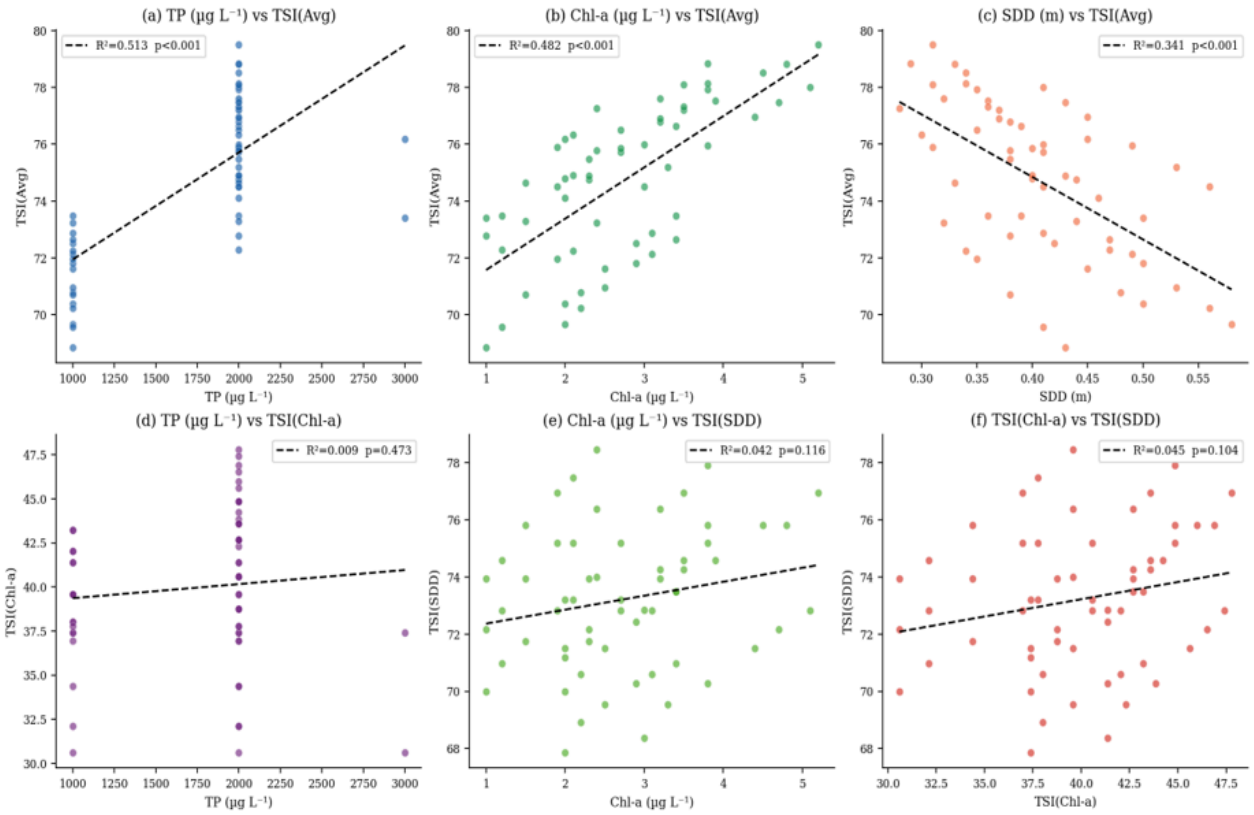

Figure 7

Multi-parameter regression scatter plots (a–f) for key variable pairs across n = 60 station-month observations. Regression equation, R², and p-value are indicated on each panel. Points coloured by station.

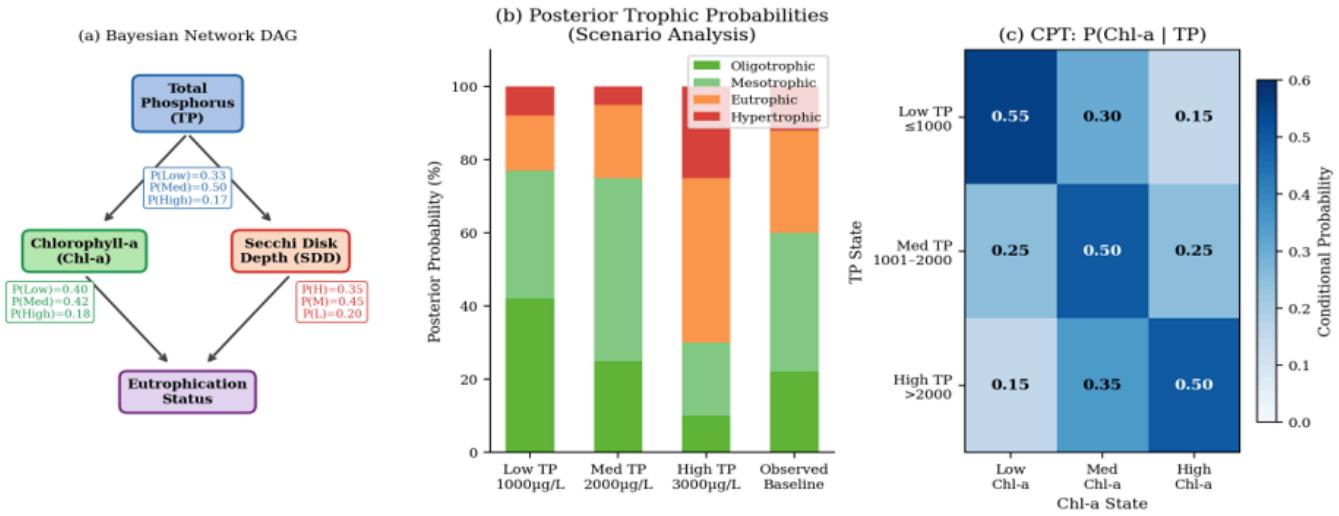

Figure 8

Bayesian Network analysis: (a) Directed Acyclic Graph (DAG) with marginal probability distributions at each node; (b) stacked posterior trophic state probabilities under four TP scenarios; (c) Conditional Probability Table (CPT) heatmap for P(Chl-a | TP).

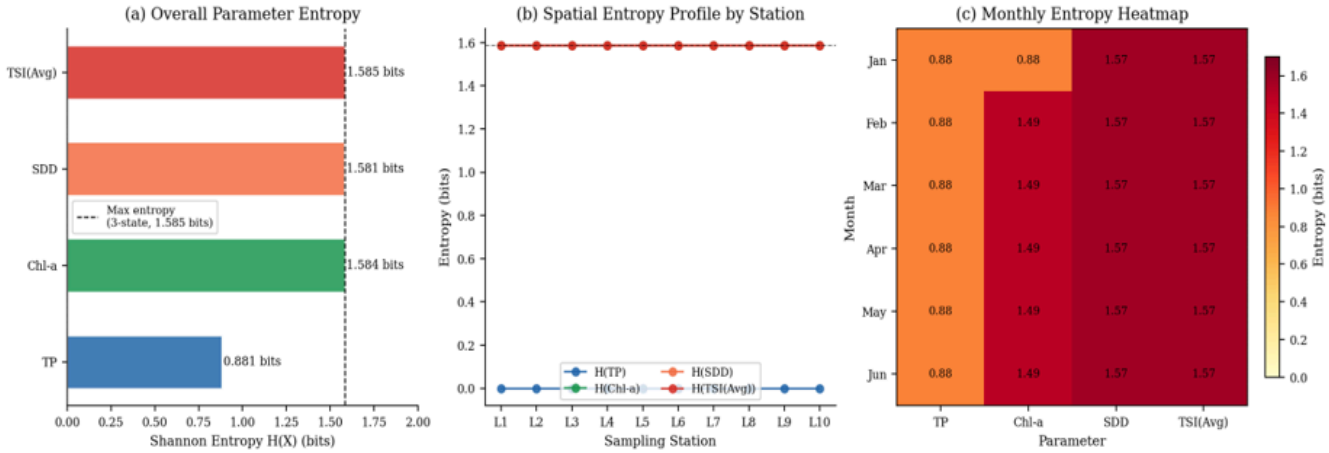

Figure 9

Shannon entropy analysis: (a) global parameter entropy with H_max reference; (b) spatial entropy profiles by station across 6 months; (c) monthly entropy heatmap showing temporal evolution of parameter uncertainty.

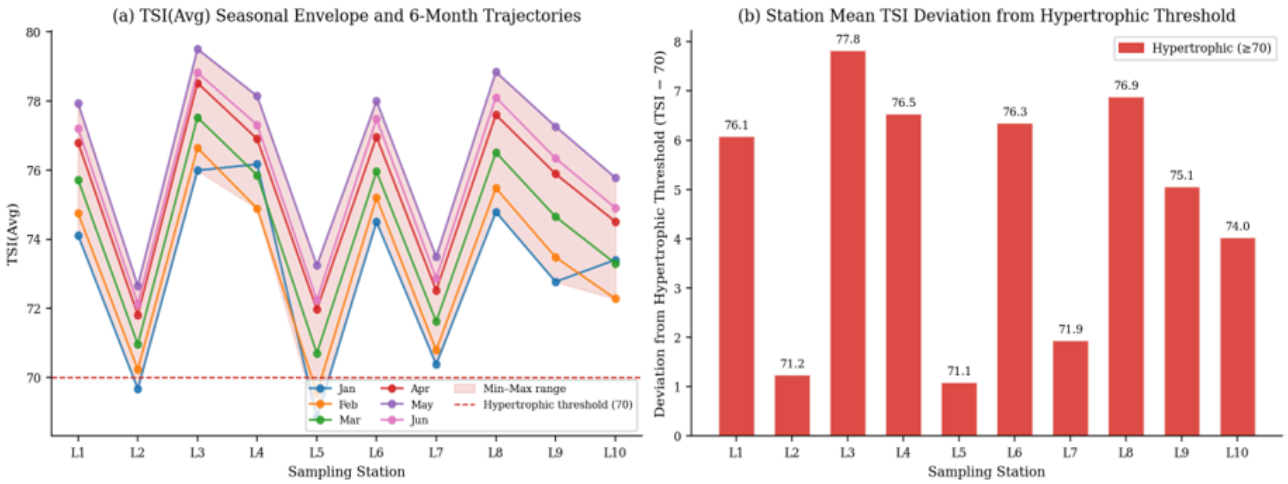

Figure 10

(a) Seasonal TSI(Avg) envelope showing min–max range and 6-month trajectories per station; (b) station mean TSI(Avg) deviation from the hypertrophic threshold (TSI = 70) with absolute mean values labelled.